

State-of-the-art

3.1. Introduction

The previous chapter exposed the reasons for the interest and application of hydrogen as an energetic vector and the introduction of electrochemical systems in the stationary and transportation energetic scene. This chapter will deepen and present a critical review of the modeling techniques proposed by other authors for each of the electrochemical systems under study, that is, fuel cells, batteries and ultracapacitors and present test platforms useful for the testing of hybrid energy systems.

3.2. Modeling techniques

As seen in the previous chapter, the operational principle of fuel cells, batteries and ultracapacitors is based on electrochemical phenomena, but other processes, such as thermal, chemical, electric, fluid dynamic, etc. are also present.

If all these phenomena should be taken into account at a time, the modeling process would result too complex and time consuming. When applying modeling and engineering processes, different approaches can be considered, depending on the final use given to the model developed. For example,

fluid dynamic, thermal, chemical and electrochemical approaches are very adequate for the development stage of electrochemical system. But for the application stage, in which the electrochemical system has to interact with the load to which it is connected, an electric modeling of the system could be more adequate. Therefore, in this chapter we will focus on those models more suitable to a seamless integration in an electric simulation tool.

Engineering models would be useless if the numerical values of their parameters could not be determined through measures. For conventional systems (electric machines, combustion engines, transformers, etc.) whose mathematical models are perfectly defined, there are set of established tests, which allow to obtain the characteristics which define the system under study.

Electrochemical systems can be also subjected to a series of tests which allow to model their electrical behavior. Unlike conventional systems, the structure and mathematical models are still not universally defined, nor the test procedure or parameter obtention univocally established. These tests can be carried out either in the time or frequency domain. One of the most extended time domain test is the current interruption test whilst the frequency domain test the electrochemical impedance spectroscopy.

3.2.1. Time domain tests

3.2.1.1. Current interruption

The current interruption test is a time domain test in which the system under study is kept at its operation point (constant current load) until it reaches stationary state. Once reached, the current load is abruptly interrupted, allowing to study the voltage evolution, depicted in Fig. 3.1. Because electrochemical systems operate in direct current (dc), this test is carried out applying a dc current and measuring the dc voltage.

It can be observed that the (discharge) current interruption causes a voltage increase until it reaches the open circuit voltage. This voltage increase is vertical during the instants after the current interruption, but changes to nonlinear until it reaches the open circuit voltage. The step voltage increment is due to ohmic voltage drop and can be represented by a resistance.

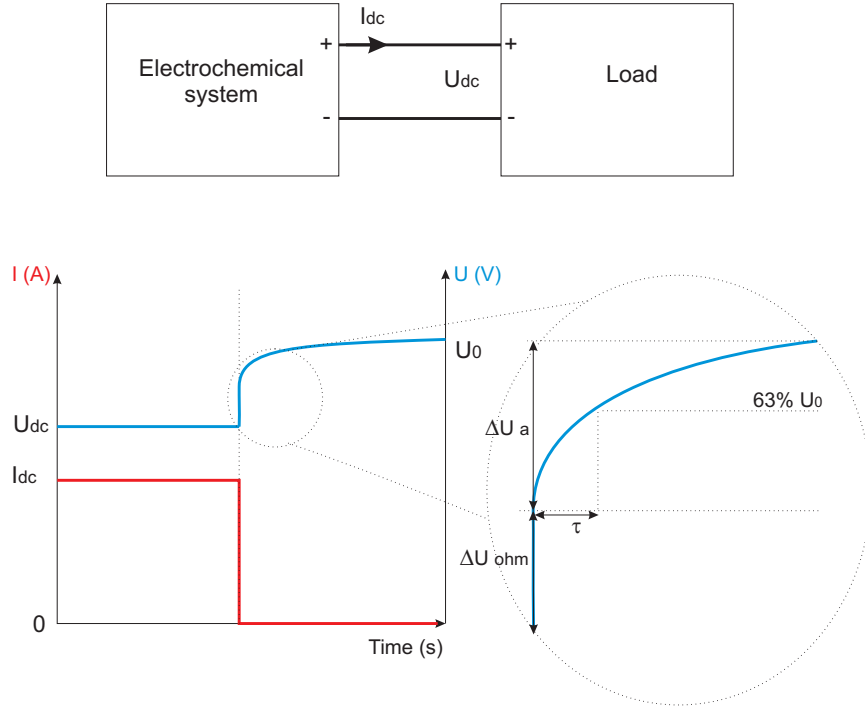


Fig. 3.1: Current interruption test

The nonlinear part can be approximated by a capacitor in parallel with a resistance (with a time constant τ). This RC network reproduces the behavior of the double layer capacitor present in electrochemical systems at the interface of the electrodes and electrolyte. The resistances and capacitance can be calculated as:

$$\begin{aligned}
 R_{ohm} &= \frac{\Delta U_{ohm}}{I} \\
 R &= \frac{\Delta U_a}{I} \\
 C &= \frac{\tau}{R}
 \end{aligned} \tag{3.1}$$

If this test is carried at different current loads I_{dc} , it is possible to analyze the dependency of each parameter with the current. Known these parameters, an equivalent circuit, depicted in Fig. 3.2, can be defined. The equivalent circuit represented includes the internal voltage E , which will depend on the electrochemical system.

The advantage of this modeling technique is its simplicity, both in setup and control. However, there are several drawbacks. The first one is that this

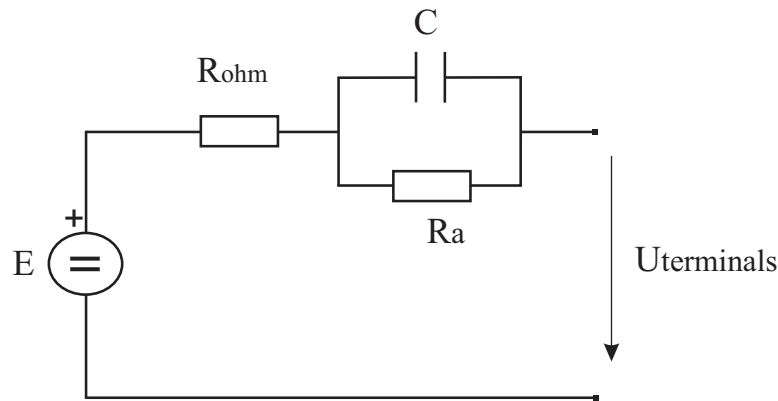


Fig. 3.2: Equivalent circuit obtained from the current interrupt test

a lumped equivalent circuit, which, for example, does not include the inductive behavior at high frequencies or the concentration voltage drop present during high load currents. Moreover, the model precision depends heavily on the correct identification of the point in which the voltage evolution changes from vertical to nonlinear. An imprecise calculation will cause the incorrect calculation of the voltage drops and the time constant. Finally, this method does not add significant information about the internal processes present in any electrochemical system.

Some examples of the application of this method to fuel cells can be found in [43], [44] and [45]. It can also be applied to batteries, but the test should be carried out for both charge and discharge processes.

3.2.2. Frequency domain tests

3.2.2.1. Electrochemical impedance spectroscopy (EIS)

The two most important differences between current interruption and EIS tests is that, whilst current interruption is carried out in the time domain and with direct current, EIS is a frequency domain test which needs the application of alternating current and voltage. One of the similarities is that EIS tests also seeks to calculate the impedance of the system under study. But the most important advantages of frequency domain tests are the richer information obtained and the simpler data processing (if the adequate software is used).

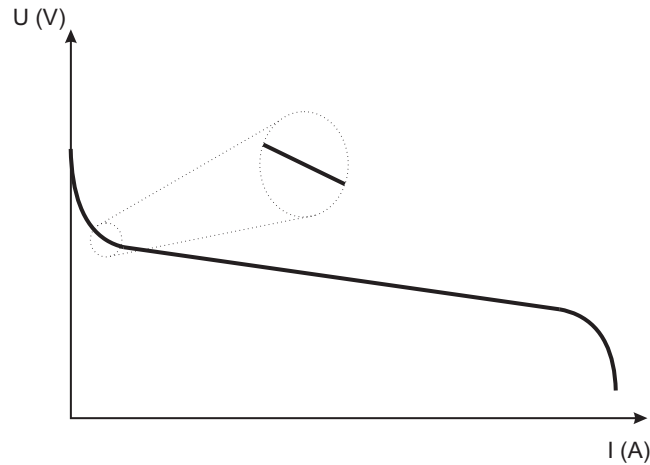


Fig. 3.3: Linearity of the characteristic curve

Electrochemical systems present a nonlinear characteristic curve. For example, Fig. 3.3 presents a fuel cell characteristic curve, which is nonlinear with a large signal analysis, but can be linearized if small variations are taken into account, as done with small signal analysis. To keep linearity during the tests, the ac signals applied are small enough (e.g. 5% of the rated voltage).

During EIS tests a small ac excitation signal (either current or voltage) is applied to the electrochemical system. This excitation signal will cause the system to react, generating an ac voltage (if the excitation signal is current) or ac current (if the excitation signal is voltage). The ac excitation signal can be applied with a fixed (not usual) or variable frequency, which in the variable case can be programmed as a sweep.

If the ac excitation signal is current, it is said to be a galvanostatic mode EIS, whilst if it is a voltage signal it is called a potentiostatic mode. The selection criteria to choose between one mode or another is frequently the control mode of the system under test. For example, the fuel cell current is more easily controlled than the voltage. Hence, it would be easier to apply a galvanostatic (current control). Supposing galvanostatic mode EIS (current control), the excitation signal can be expressed as:

$$I(t) = I_0 \cdot \cos(\omega \cdot t) ; \quad \omega = 2 \cdot \pi \cdot f \quad (3.2)$$

Where I_0 is the signal amplitude and f the signal frequency. Supposing that the system displays a linear behavior, the resulting ac voltage is:

$$E(t) = E_0 \cdot \cos(\omega t - \varphi) \quad (3.3)$$

φ is the phase at which the current signal is shifted, whilst E_0 is its amplitude. Known both the voltage and current, the complex impedance can be calculated as:

$$Z = \frac{E(t)}{I(t)} = \frac{E_0 \cdot \cos(\omega \cdot t - \varphi)}{I_0 \cdot \cos(\omega \cdot t)} = Z_0 \cdot \frac{\cos(\omega \cdot t - \varphi)}{\cos(\omega \cdot t)} \quad (3.4)$$

Electrochemical systems generate direct current, therefore, it is unavoidable to have both dc and ac signals while carrying out EIS tests. The dc level is used to keep the electrochemical system at its operation point, but it is not considered for the impedance calculation, in which only the ac signals are involved. This implies that the dc level must be rejected before the ac impedance is calculated. A diagram explaining the whole process is presented in Fig. 3.4.

EIS tests can be carried out with off-the-shelf equipment: electronic load, signal generator and voltage and current transducers. However, the subsequent impedance calculation and model extraction is time consuming and complex. Therefore, it is recommendable to use an impedance analyzer, which generates the excitation signal and calculates the complex impedance by measuring the current and voltage.

However, impedance analyzers are equipments more focused to test passive elements, which can be correctly characterized with the 60 mA current and 45 V threshold. However, the current limit is clearly insufficient for active elements, which can reach hundreds of amperes. This low current threshold forces the use of other equipments along with the impedance analyzer, such as potentiostats, which are able to absorb higher dc currents. However, potentiostats present a maximum of 100 A (the most expensive equipments, less than 40 A the rest), which is still a low value for testing, e.g. ultracapacitors.

After the EIS test is carried out, the data must be processed. Normally the impedance analyzer includes a software package to do it. The data is

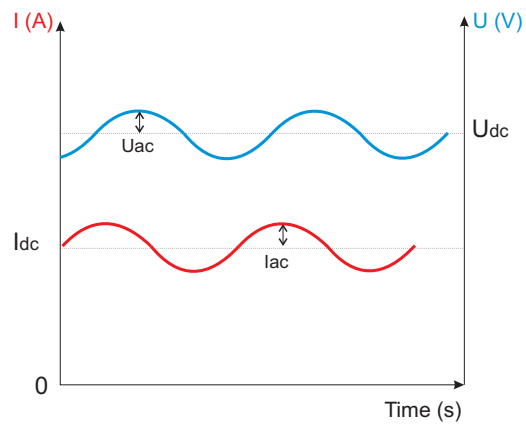
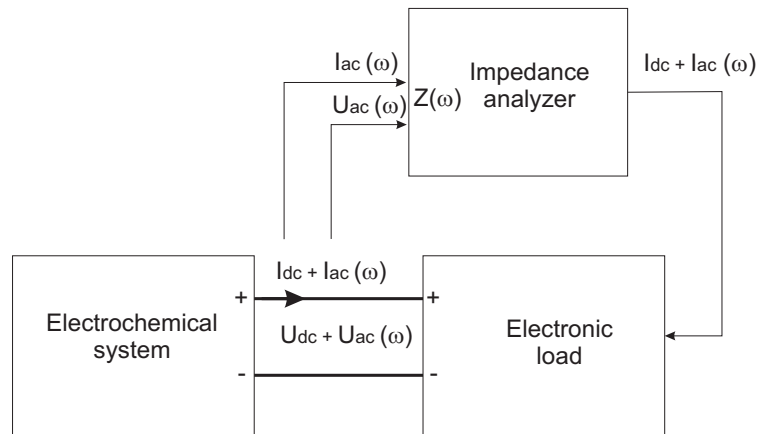


Fig. 3.4: EIS test diagram

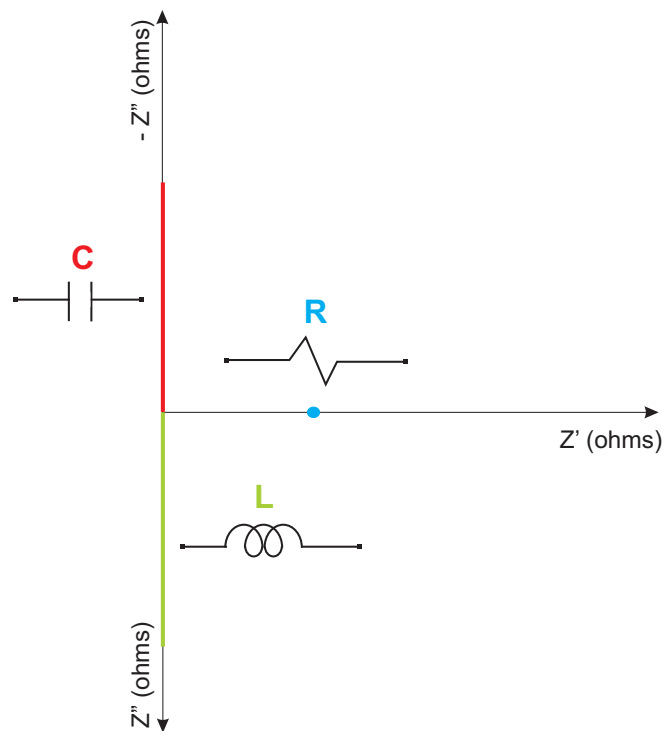


Fig. 3.5: Nyquist plots for ideal elements

rendered in a text file, which is translated by the software to a Nyquist and Bode plot. Knowing these two plots, especially the Nyquist plot, the user can define an equivalent circuit, which the programme fits to the experimental results, as shown in Fig. 3.5.

The most frequently used elements are resistances, capacitors and inductances. Fig. 3.5 presents the Nyquist representation for each of these systems. The abscissa axis represents the real part of the complex impedance (Z'), whilst the ordinate axis is the imaginary part (Z''). To facilitate the interpretation of the Nyquist plots, the upper part of the imaginary plot corresponds to the negative imaginary part ($-Z''$).

$$Z = Z' + jZ'' \quad (3.5)$$

The resistance is represented by a point on the abscissa axis, with no imaginary part. Ideal capacitances or inductances correspond to vertical lines on the diagram. These type of ideal elements are rarely, if ever, found. It is more frequent to encounter real systems, which include the association of

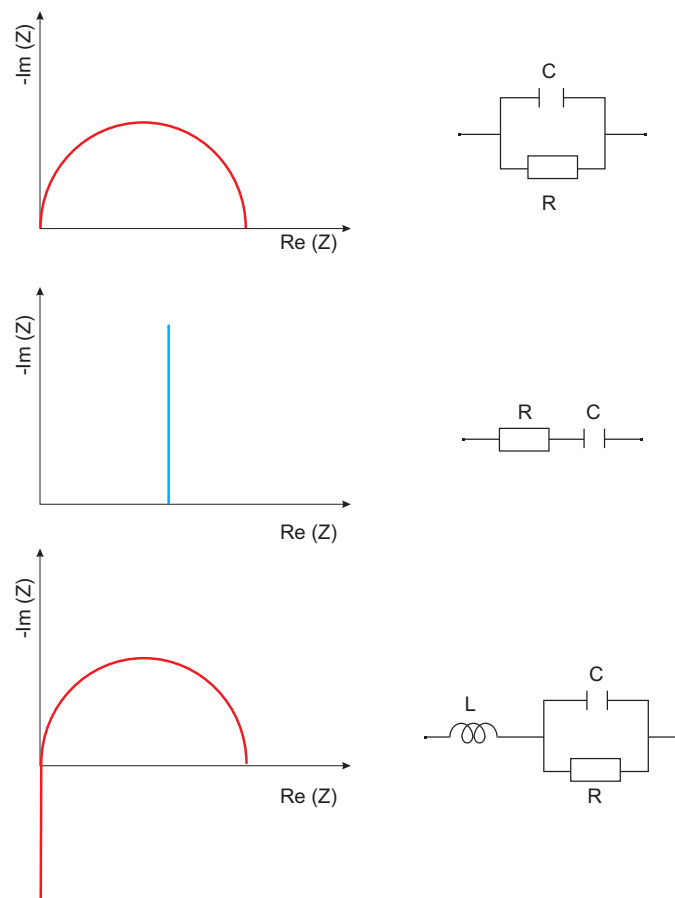


Fig. 3.6: Nyquist plots for combined ideal elements

two or more of these elements, as presented in Fig. 3.6.

For electrochemical systems, classic electric elements (resistances, capacitors and inductances) may not be enough to represent their internal behavior, due to, for example, diffusion phenomena. Most electrochemical systems use porous or rough materials for the electrode manufacture, which affect the diffusion of reactants. As stated by Barsoukov [46], diffusion causes an effect similar to a finite transmission line: the answer of the output to an electric stimulation is delayed, compared to the input. Therefore, the electrochemical system will present a distributed equivalent circuit. The exact impedance cannot be represented as a finite number of equivalent circuits, but for computational sake, it is normally limited to a finite number.

In order to represent this distributed effect, it is possible to find distributed elements, such as infinite and finite Warburg impedances, constant

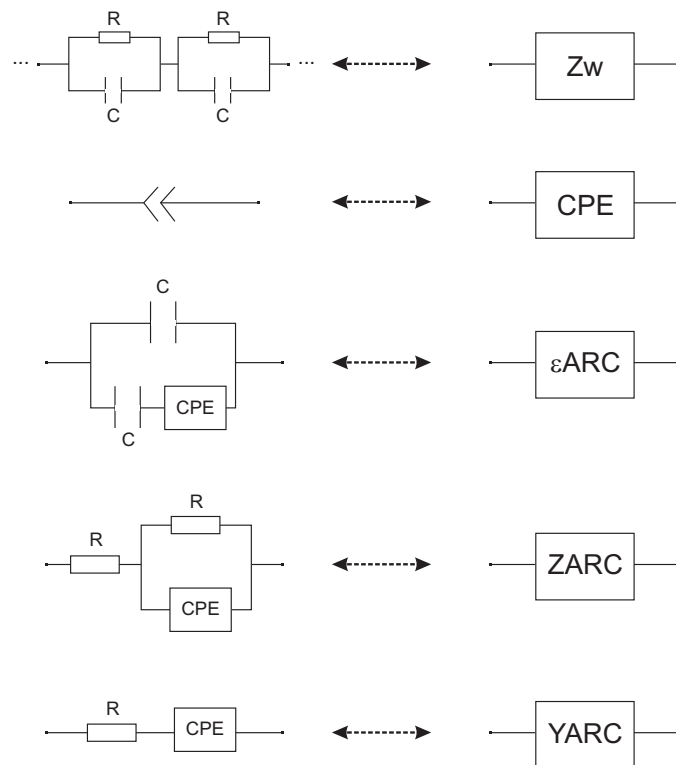


Fig. 3.7: Nyquist plots for diffusion elements

phase elements, ZARC or YARC, among others. The finite Warburg (Z_w) impedance does not correspond to an ideal impedance, such as resistance, capacitance or inductances. It is therefore simulated through an equivalent circuit of distributed RC networks, which can have a finite or infinite number of RC networks.

Another diffusion element is the constant phase element CPE. It can be used combined with other elements. When used in parallel with resistances it can reproduce a depressed semi-circle with the center lower than the abscissa axis. The CPE-R with another resistance in series result in a ZARC (ARC in the Z plane) element. The YARC (ARC in the Y plane) is obtained with the series connection of a CPE and resistance, as depicted in Fig. 3.7. This CPE element can also represent the electrode roughness, due to the fact that electrodes may present a fractal dimension (between 2 and 3 dimensions). It is also considered to represent the inhomogeneous distribution of reactants on the surface or the varying thickness and composition [46].

3.3. State-of-the-art of the modeling of electrochemical systems

3.3.1. Fuel cells

As commented earlier, there are a series of test methods which can be applied to characterize a fuel cell. A revision of these methods was done by Page [47] and Wingelaar [48].

One of the classic models, presented by Amphlett [49] in 1996, is a mechanistic model which takes into account mass and heat transfer in a PEM fuel cell. Later, in 2002, Pukruspan [50] presented a more complete model which included models for the auxiliary systems (compressor, etc.) and used the mass conservation principle and thermodynamic equations to calculate the flow of reactants through anode and cathode. It is an interdisciplinary model, which is more focused on the fuel cell system, rather than on the fuel cell stack.

Electric models are normally more focused on the fuel cell stack model, which is the element which generates the electric power. A classic model for the fuel cell stack is the one developed by Larminie [35] in 2000 and developed by Pathapati [8] in 2005. Both authors used models which included equivalent circuits, as the one depicted in Fig. 3.8, which were able to reproduce the fuel cell electric behavior. The equivalent circuit is the same as the one obtained by current interruption, that is, a lumped equivalent circuit. Despite the fact that Pathapati presents a dynamic model, it is validated with a nearly steady state current profile, so no information about the model behavior during abrupt loads is given.

In 2005 Wang presented a dynamic model programmed in Matlab/Simulink and PSPICE [51]. The equivalent circuit presented is the same as the Larminie and Pathapati circuit. But Wang carried out a series of experimental tests which allowed him to obtain the dependency of each parameter (resistances, voltage, etc.) with current and temperature. However, he did not mention the tests he carried out to obtain these relationships, so even though it is a highly referenced paper, it still has to prove how parameters were obtained.

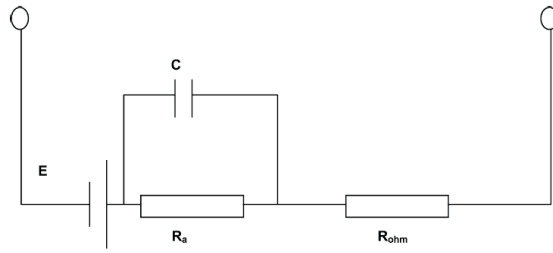


Fig. 3.8: Equivalent circuit presented by Pathapati and Larminie [8]

Moreover, he did not include a temperature model, even though temperature is a key parameter which influences the internal voltage of a fuel cell. Other authors, as Zhang [52] and Soltani [53] do include it. In comparison to Pathapati, Wang did apply a dynamic current profile in order to validate the model voltage dynamically.

The development of more detailed equivalent circuits needs EIS tests, such as those applied by Yuan in [54] and [55]. An analysis of the application of EIS to fuel cells was done by Parthasarathy in [56]. Yuan presented the experimental procedure for the application of EIS tests for individual cells and stacks. He discussed which should be the relationship between the ac and dc signal amplitude. He investigated ac signals with an amplitude between a 1 and 15 % of the dc signal amplitude and concluded that for amplitudes smaller to a 5 % the data points were too scattered due to noise, whilst amplitudes larger than 5 % distorted the Nyquist plot at low frequencies.

He also mentioned two different equivalent circuits which could be fitted to the data obtained after the EIS tests, but did not present its equations or justify the election of those parameters. The most striking difference with the circuit mentioned up to this point is the substitution of the capacitors by constant phase elements CPE. However, he did not demonstrate the suitability of its use compared to a capacitor. Finally, he did not validate the circuits mentioned as his work is more centered on the EIS tests itself, rather than on the obtention of a dynamic model.

Other authors, as [9] and [57] keep the capacitor, but include the diffusion in the models by adding a Warburg impedance in series with the resistance of the RC network, as shown in Fig. 3.9, forming a so called Randles circuit.

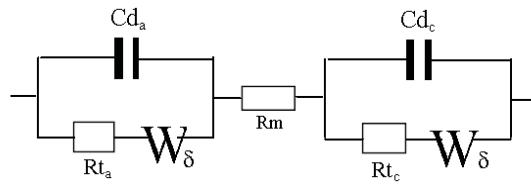


Fig. 3.9: Equivalent circuit presented by Garnier and Laffly [9]

Similarly to the CPE, the Warburg impedance has no electric equation, so it must be fitted to another element which can be described by a single or combined number of electrical components. The Warburg is normally substituted by a series connection of RC networks. The number of RC networks connected in series depends on the user (Garnier [9] used 10). However, this increases the number of differential equations which must be solved to calculate the output voltage.

Other authors which apply EIS to PEM fuel cells are Brunetto, Cooper and Zhu. Brunetto [58] carried out the EIS tests after keeping the fuel cell 5 hours in its operation point, in order to guarantee the fuel cell stationary state. The equivalent circuit is similar to the one used by Garnier, but without the Warburg impedance. He took into account the temperature effect, but did not model it. As commented with Wang, the temperature affects the fuel cell internal voltage, and should therefore be taken into account.

Cooper [10] carried out a revision of the electrical tests which can be carried out on fuel cells, and applied each of them, but did not present a critical comparison. He carried out EIS tests from 1 Hz to 10 kHz and presented the Nyquist plot obtained after tests, in which the fuel cell presented a capacitive behavior at 20 kHz. But other authors, as Zhu [59], actually found inductive behavior at 10 kHz. The equivalent circuit presented by Cooper is a transmission line model formed by resistances and capacitors, as shown in Fig. 3.10.

Other authors develop the fuel cell models as transfer function, as done by Boccaletti [60], Soltani [53] and Yalcinoz [61]. Only Soltani experimentally validated his model.

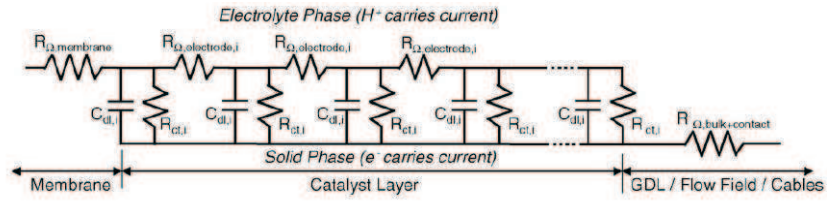


Fig. 3.10: Equivalent circuit presented by Cooper [10]

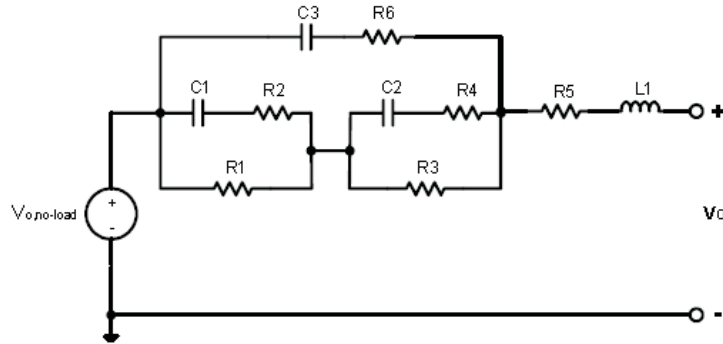


Fig. 3.11: Equivalent circuit presented by Choi [11]

Finally, Choi [11] developed a dc and ac equivalent circuit. The ac equivalent circuit was obtained after EIS tests. He proposes a per-unit system for the fuel cell, by using a base power, voltage and current which is a useful tool when connecting fuel cells to other power electric systems. However, he did not develop the idea by using the inverter as a base voltage transformer or by comparing the different fuel cells he models in per-unit values. Moreover, he did not include a base frequency for the ac equivalent circuit, shown in Fig. 3.11, or experimentally validate the developed model.

As a conclusion, multiple models have been presented for a fuel cell simulation. The equivalent circuits presented generally include similar elements. However, those who have included diffusion elements, such as CPE have not demonstrated its adequacy compared to capacitors. Moreover, of those authors who obtained the models through EIS tests, some studied the temperature effect on the fuel cell impedance, but did not develop a temperature model. This temperature model is necessary to calculate the fuel cell internal voltage. Also, the direct comparison of parameters for similar fuel cells is difficult due to the absolute value approach. This problem could be solved by using a per-unit approach, as done by Choi. However, Choi does not totally

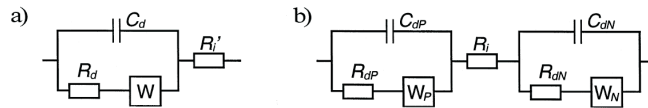


Fig. 3.12: Equivalent circuit presented by Karden [12]

define the base system, as he does not include a base frequency or comment the per-unit approach adequacy when connecting the fuel cell model with other power electric elements.

3.3.2. Batteries

One of the most relevant contributions to batteries was made by Peukert in 1897 [62]. Peukert carried out constant current tests to lead-acid batteries and discovered a relationship between the battery capacity, current and discharge time. This is a useful tool to know, e.g. the remaining capacity after a certain discharge time has gone by. The Peukert equation has been studied more recently by Doerffel [63].

The Electrochemical Energy Conversion and Storage System research group at the ISEA (Institute for Power Electronics and Electric Drives), Aachen University (Germany) is a reference for the modeling of electrochemical systems, specially batteries. In 2000 Karden [12] presented a method for measuring and interpreting battery impedance. They developed their own impedance analyzer and carried out galvanostatic EIS tests during continuous discharge and mini-cycles for different states of charge. They did not focus specifically on the development of an equivalent circuit, however, they did propose the one presented in Fig. 3.12. This figure presents two different equivalent circuits. Both present Warburg impedances, in order to reflect the diffusion at low frequencies. The difference between them is that one includes just one RC network, whilst the other presents two (one RC network per electrode). Later, he extended this analysis to other electrochemical systems [64].

Other authors, such as Tenno studied the relationship between the battery impedance and its characteristics [65]. He used an equivalent circuit similar to the two RC network model presented by Karden. But Tenno did

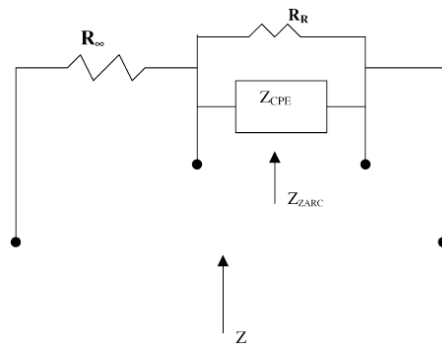


Fig. 3.13: Equivalent circuit presented by Nelatury [13]

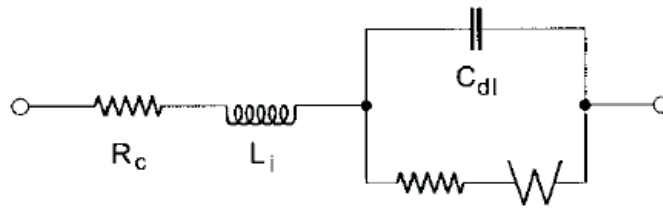


Fig. 3.14: Equivalent circuit presented by Baert [14]

not take into account the diffusion phenomenon.

In 2002 Nelatury [13] presented an equivalent circuit with just one network, but substituted the capacitor by a constant phase element CPE, as shown in Fig. 3.13. The R-CPE combination is also called ZARC, which is the expression he used. However, he did not validate the equivalent circuit presented. Other authors, like Buller [66], also used ZARC elements, but applied to Li-ion batteries.

Baert [14] included an inductance in series with the series resistance and RC network with a Warburg impedance, which is depicted in Fig. 3.14. The inductance he included models the inductance of the conducting path, which he considered constant for any state of charge. He proposed to center the attention on the resonance frequency (frequency at which the battery impedance is purely resistive) because of the slow phenomena on the electrodes, which are unable to follow high frequency excitation. He therefore simplifies the previous equivalent circuit to a series RLC circuit.

Another author who included the inductance is Salkind [15]. He carried

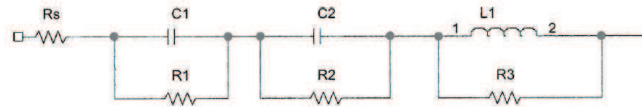


Fig. 3.15: Equivalent circuit presented by Salkind [15]

out EIS tests for two different batteries between 0.65 Hz and 65 kHz. Fig. 3.15 presents the equivalent circuit he proposed. It includes the series resistance and the two RC networks, as well as the inductance, but with a parallel resistance inductance. He did not explain the reason for using this parallel resistance inductance.

In 2005, Thele [67] presented a battery model which was developed in a hybrid frequency and time domain. The reason for this approach is that any model obtained with EIS tests is a good approach for highly dynamic operation, but loses precision when longer processes need to be simulated (transport of sulphuric acid). However, to carry out this hybrid modeling it is necessary to know the thickness, porosity and geometric surface of the electrodes, values which are very difficult to obtain.

Thele, in 2008 developed a voltage behavior for Ni-Mh batteries [16] which can also be applied to lead-acid batteries. The equivalent circuit used is shown in Fig. 3.16 and includes a Warburg impedance in series with the rest of elements. Thele also presented the hysteresis effect of the open circuit voltage (*OCV*) for Ni-Mh batteries, in which the *OCV* presents different evolution with the state of charge depending on the nature (charge or discharge) of the process. This hysteresis curve is depicted in Fig. 3.17. Even though the hysteresis effect is not difficult to measure, it is seldom taken into account by most authors. However, the difference between charge and discharge curves of the hysteresis curve is sufficiently different to affect the final model precision.

Finally, there are authors, such as Huet [68], who are exclusively interested on the battery high frequency resistance, which is the battery impedance for the resonance frequency. He concluded that this resistance depends on the state of charge, but not on the current. Moreover, he investigated if this resistance could be an indicator of the battery state of charge, but concluded that it was not a reliable for state of charge monitoring. Huet had previously

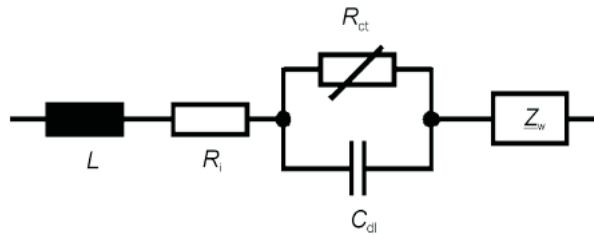


Fig. 3.16: Equivalent circuit presented by Thele [16]

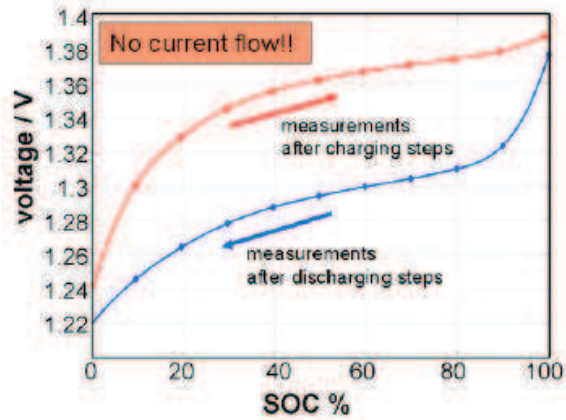


Fig. 3.17: Hysteresis effect on the battery open circuit voltage presented by Thele [16]

(1998) studied different ways to determine a battery state of charge and health [69].

The state of charge measurement, essential for the battery operation life, is a complex task due to all the chemical phenomena which takes place in a battery. Some authors, as Viswanathan [70], investigate the relationship between the charge transfer resistance (part of the RC network) and capacitance with the state of charge. They concluded the charge transfer resistance and capacitance increased for increasing states of charge. This relationship between the capacitance and state of charge was also observed by Tenno [65]. More recently, Hariprakash [71] and Blanke [72] have also studied the use of impedance measurements to calculate the battery state of charge and state of health.

Once all these battery models have been analyzed, it is surprising to find that only Thele takes into account the hysteresis effect on the battery internal voltage. Also, no author comments the difficulties present when comparing the different models for similar batteries. Even for the same technology and depending on the battery capacity and voltage, the parameters can vary orders of magnitude, which makes it difficult to directly compare models. This problem could be overcome with a per-unit comparison, but has not been found in literature.

3.3.3. Ultracapacitors

If compared to batteries, or even fuel cells, the modeling of ultracapacitors is less mature. Some authors which explain the ultracapacitor technology and limitations are Burke [42] and Conway [73]. The modeling techniques are the same as used for batteries or fuel cells, but present particular characteristics, as explained below.

In 2000 Zubieta presented the characterization of ultracapacitors for power electronic applications [17] in the time domain. He modeled the ultracapacitor as a three time-constant circuit formed by capacitors and resistances, as shown in Fig. 3.18. He reflected the dependency between capacitance and

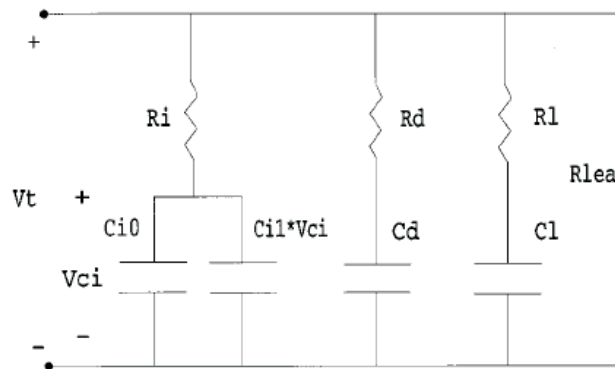


Fig. 3.18: Ultracapacitor equivalent circuit presented by Zubieta [17]

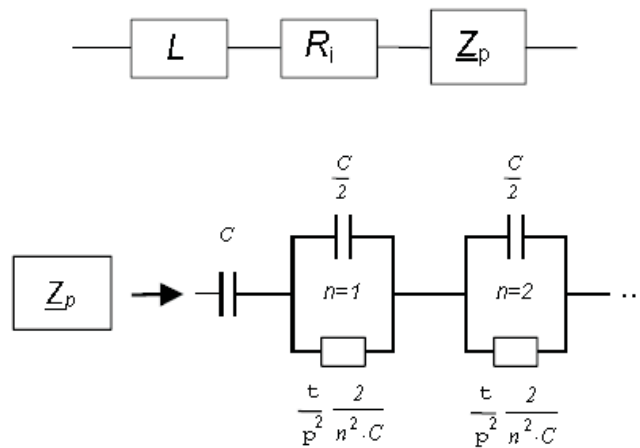


Fig. 3.19: Ultracapacitor equivalent circuit presented by Buller [18]

voltage with variable capacitors. He modeled 470 F and 1500 F capacitors by charging and discharging them and relating each branch parameters to the terminal voltage and time.

In 2001, Buller modeled the dynamic behavior of a 1400 F ultracapacitor through EIS tests [18]. He used an impedance analyzer developed at Aachen for battery testing. The EIS test were galvanostatic, with a frequency sweep between 10 μ Hz and 6 kHz. He did not specify the ac current amplitude, just indicated it was a small ac current. However, ultracapacitors need large currents to cause a small voltage ripple. He obtained an equivalent circuit formed by an inductance, a series resistance and a series connection of RC networks, as it can be seen in Fig. 3.19.

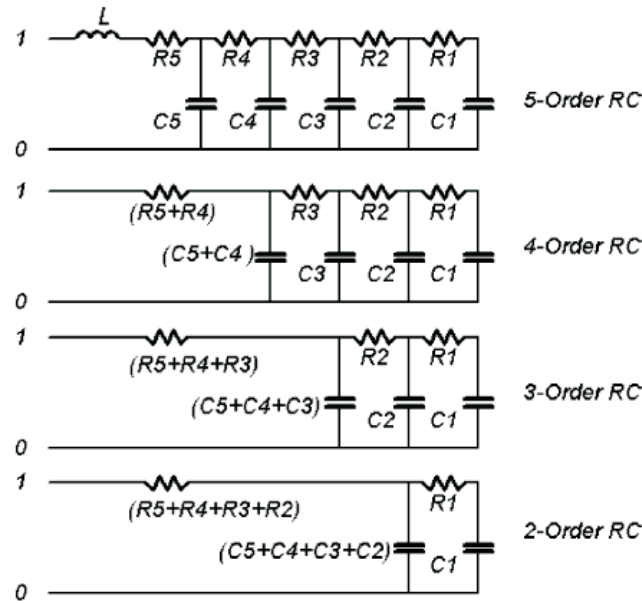


Fig. 3.20: Ultracapacitor equivalent circuit presented by Dougal [19]

During 2003 Lufrano also carried out EIS tests on ultracapacitors. But the main difference is that he did it in potentiostatic mode, with a 20 mV ac voltage excitation. He studied the evolution of the capacitance for different active materials with frequency, but did not specify a particular equivalent circuit.

Furthermore, authors do not agree on the number of RC networks that should be used. Dougal [19] presented the circuit shown in Fig. 3.20 to which he applied an automatic order selection method, changing the circuit order by taking into account different capacitors, depending on the phenomena it reflects. Leaving apart the inherent complexity of the method, the capacitance validation he presented does not follow the measurements trends and differs from one to three orders of magnitude. Moreover, the model voltage is not validated with experimental data.

Lajnef obtained a similar circuit to the one presented by Dougal, but with a fourth order circuit [74]. He used both current tests and frequency analysis. With the current tests he characterized the internal resistance and average capacitance. For the frequency analysis he used potentiostatic EIS tests between 10 mHz and 1 kHz, however he did not detail the ac voltage

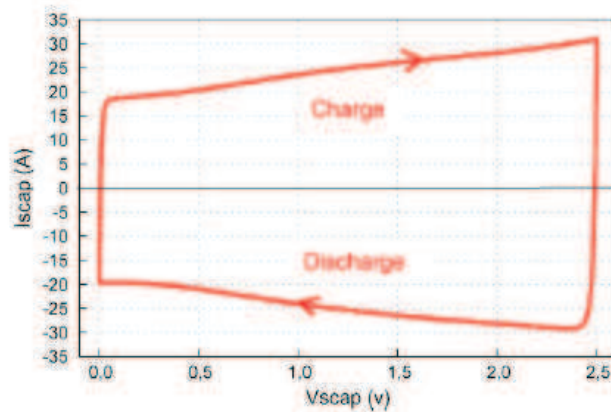


Fig. 3.21: Ultracapacitor voltamogram presented by Lajnef [20]

ripple amplitude. He validated the model experimentally, but recognized the inability of the model to take into account the voltage dependence of the capacitors. He later completed this work verifying the difference in the internal resistance during charge and discharge. Also, he presented the different methodologies used to characterize ultracapacitors, as the voltamogram presented in Fig. 3.21 [20]. He also participated in the study of supercapacitor ageing carried out by Briat [75]. At the end of 25,000 tests they observed an increase in the ultracapacitor impedance and a loss of capacitance. He later continued with this research in [76].

To consider the temperature effect, Michel [77] observed that capacitance was reduced at freezing temperatures, due to the viscosity of the electrolyte at such low temperatures. He also observed a considerable increase of the internal resistance at these temperatures, for exactly the same reason. This is one of the arguments used by Rafik [21] for not taking into account the effect of temperature on the capacitance for positive temperatures. He used the equivalent circuit depicted in Fig. 3.22 to model a 2600 F with potentiostatic EIS tests. He carried out these tests with a 10 mV ac ripple (0.4% of the dc voltage) superimposed to the dc voltage.

To conclude, there is a considerable percentage of models that have not been validated, and whose applicability may be questioned. Moreover, some authors do not include how the EIS tests were carried out. Even if some commented the ac ripple amplitude and frequency range, in most cases nothing

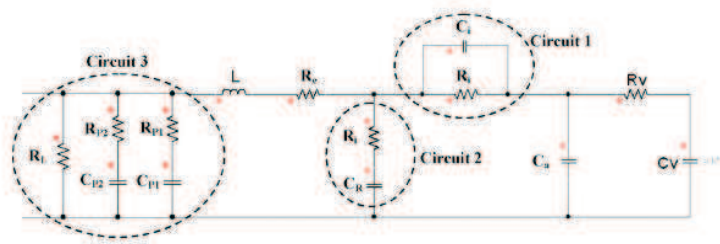


Fig. 3.22: Ultracapacitor equivalent circuit presented by Rafik [21]

is said about the impedance analyzer current limit or experimental setup and test procedure. This may be due to the fact that the ultracapacitors modeled do not present a very large capacitance. Finally, no author explains the model implementation and simulation, which is not straightforward because all the parameters depend on the voltage instead of on the current, as it is the case for fuel cells and batteries.

3.4. State-of-the-art of the simulation of hybrid electrochemical systems

The complete hardware setup of hybrid systems presents some drawbacks which cannot be ignored, such as high costs of the elements under test, the infrastructure and security requirements (especially for a hydrogen storage and supply system) and the complexity associated to the performance of the test when a high number of elements are involved. The other option is the pure simulation, which presents a lower cost, but presents the disadvantage of no real tests, to validate or confirm the system modeled. An intermediate solution between the two previous approaches is the hardware-in-the-loop (HIL) simulation, in which one or several devices of the system are used instead of their simulated models. This type of simulation lowers the cost and reduces the infrastructure needed.

In 1997 Maclay [78] underlined the usefulness of this simulation tool, which allows to mix both simulated and hardware systems. It is specially useful for hybrid energy sources and electric drives, as explained and classified by Bouscayrol [79].

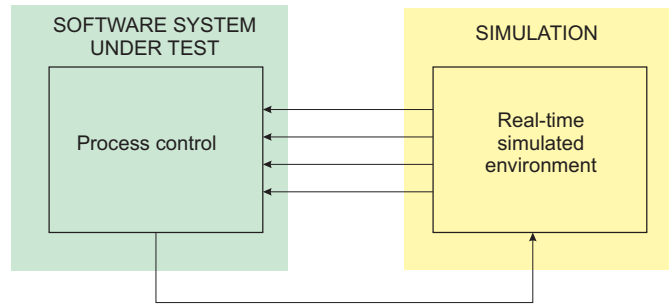


Fig. 3.23: Signal level HIL simulation

This classification is done considering the type of signal which interacts between the simulated and hardware system. The first type is the signal level HIL simulation. As seen in Fig. 3.23 the hardware element is a control scheme or similar, which interacts through control signals with the simulated environment (electric machine, mechanical load or power electronics). In this case, a control scheme can be tested without actually setting up a complex and expensive laboratory test bench due to the fact that the control schemes only need a processor and computer and the system which controls is also simulated through software. This approach has been applied, e.g. for power electronics testing [80].

The next HIL simulation level is the power level. In this case one of the simulated systems is substituted by the hardware real system, whilst the rest remains simulated. Now the simulated and hardware system also require power signals, as shown in Fig. 3.24. This is an increasingly used approach for highly complex systems, such as vehicles or electric drives. For example, Ren tested an all electric ship, with the electric machines and converters as real hardware. The simulated element is an electric power system (up to 756 nodes). The interface between simulated and hardware is done through a 5 MW power interface system, which is able to reproduce the voltage and current waveforms generated by the simulated power system. In this way, they could test the all electric ship propulsion without actually using a real ship, which is an extremely expensive option.

Moore [23] applied this simulation technique to PEM fuel cells, as presented in Fig. 3.26. In this case, Moore simulated the whole vehicle (electric

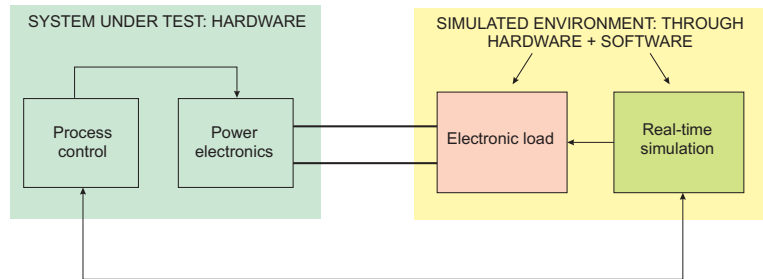


Fig. 3.24: Power level HIL simulation

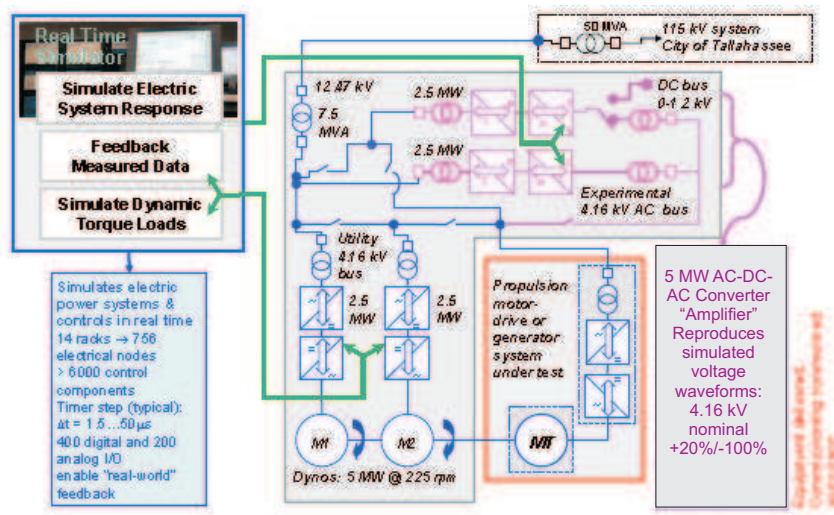


Fig. 3.25: HIL test bench for all electric ship simulation [22]

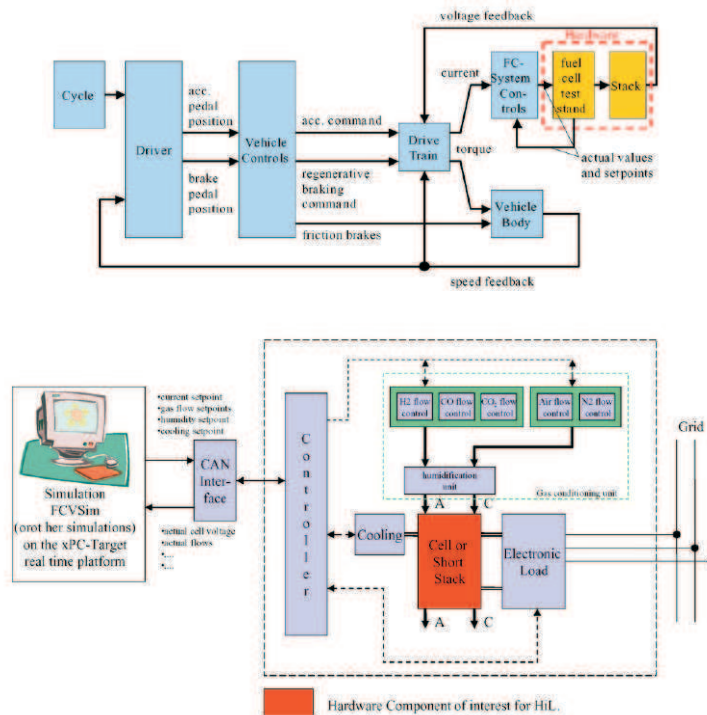


Fig. 3.26: HIL simulation presented by Moore [23]

machine included) and kept the fuel cell as the hardware element. The approach chosen by Moore is interesting due to the fact that he simulated the vehicle. However, the particular application is not realistic due to the fact that fuel cells cannot follow the vehicle load profile during acceleration or uphill, and therefore need high power storage systems.

The last HIL simulation level is the mechanical level, where the whole drive (control, power electronics and electric machine) is hardware. The simulated load is setup with a mechanical load or another electric machine. Therefore, both hardware and simulated elements interact mechanically, through the shaft, as depicted in Fig. 3.27. This mechanical level simulation can be interesting for vehicular applications, such as the diesel hybrid (battery) vehicle case carried out by Trigui [24]. In this way he could study the fuel consumption for different driving cycles. Due to the high cost and complexity of a real diesel hybrid vehicle, they simulated the vehicle chassis, driver, control, gear box and clutch, as seen in Fig. 3.28. The hardware elements were the internal combustion engine (ICE) and electric machine, with the necessary clutch and power converters. This setup is particularly useful for

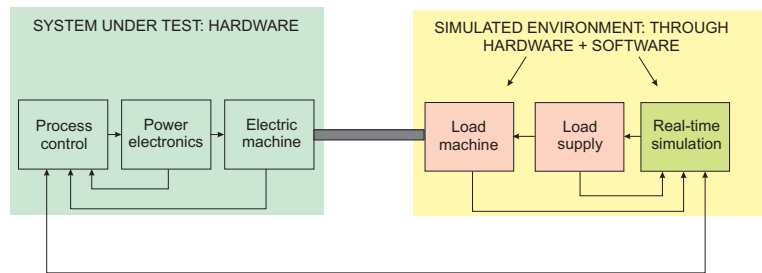


Fig. 3.27: Mechanical level HIL simulation

ICE based vehicles, but it is a very complex and expensive setup, which is specifically focused for vehicular applications, and hence presents a low flexibility for other types of loads or vehicle topologies, such as hybrid electric vehicles.

Another vehicular example of a HIL simulation, this time a power level HIL, is the hybrid electric vehicle simulated by Cheng [25]. He simulated a fuel cell/ultracapacitors vehicle with a simulated source for the fuel cell and real ultracapacitors. Due to the high cost and complexity of the vehicle, he simulated the vehicle through an electric machine connected to another electric machine connected to the dc bus, as shown in Fig. 3.29. He carried out the simulation of a normalized driving cycle. Even though this setup is simpler and with lower cost if compared to a real vehicle, the vehicle simulator is unnecessarily complex. Timmermans [81], who collaborated with the same authors as Cheng, presents similar work to the presented by Cheng, but more focused on the test bench development. In both cases, the presence of the electric machines increases the total cost and complexity. Moreover, the systems are specifically scaled for the particular case studied.

Schupbach [26] also presented a mechanical level HIL simulation for testing power trains of electric vehicles. However, he focused on the electric machine and used the Advanced Vehicle Simulator ADVISOR to simulate the energy sources. ADVISOR was developed by the National Renewable Energy Laboratory in USA (NREL) and is a Matlab/Simulink based platform which allows to simulate a wide range of commercial electric vehicles. Fig. 3.30 presents the HIL developed. Finally, another mechanical HIL simulation is the one presented by Winkler [27], who used the software Modelica/Dymola software and is also more centered on the mechanical part of the power train,

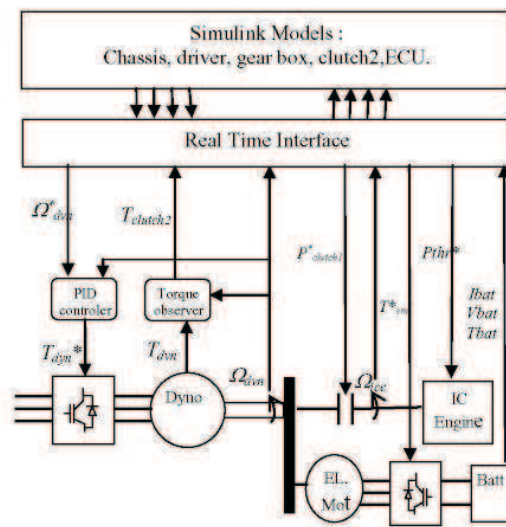
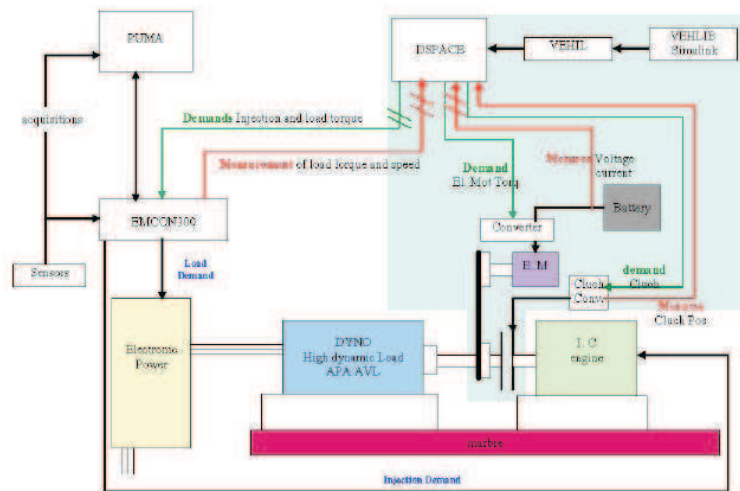


Fig. 3.28: HIL test bench for diesel hybrid vehicles [24]

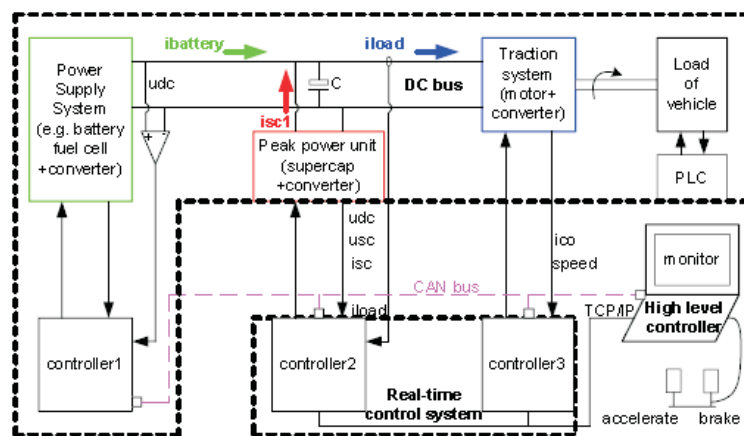


Fig. 3.29: HIL simulation presented by Cheng [25]

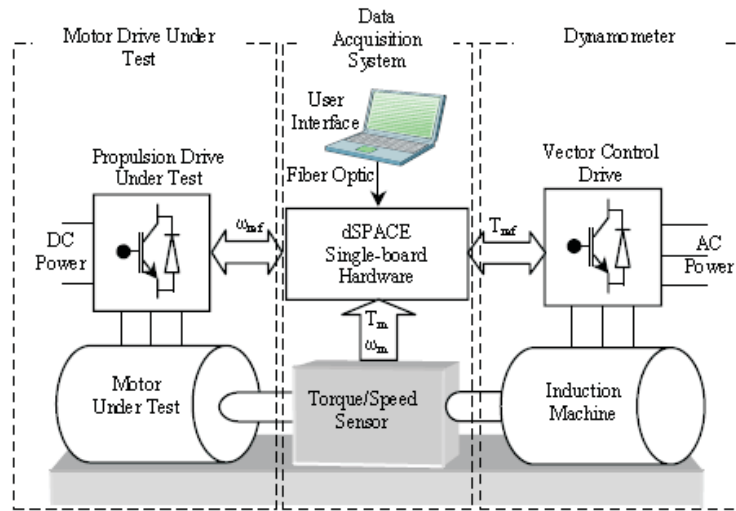


Fig. 3.30: HIL simulation presented by Schupbach [26]

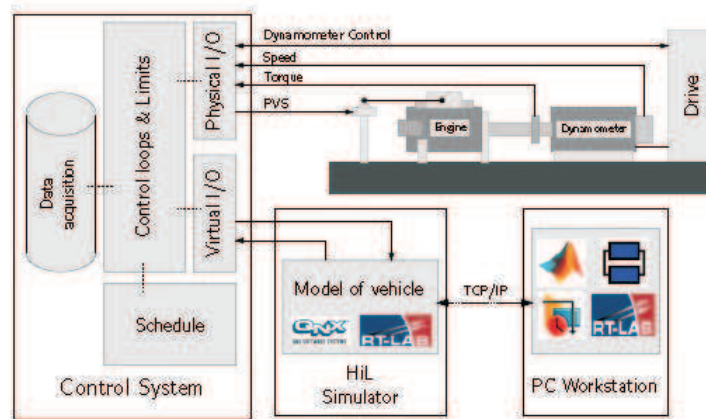


Fig. 3.31: HIL simulation presented by Winkler [27]

as it can be observed in Fig. 3.31. In both cases, the authors are very focused on the mechanical part of the power train, and not on the energy sources.

It can be concluded that most works use mechanical level HIL simulation, which is costly and complex due to the electric drives. Moore presented a power level HIL simulation for a fuel cell vehicle, with a completely simulated vehicle. However, his approach is not realistic as the fuel cell cannot supply the necessary power during acceleration. It would have been more interesting to test a hybrid electric vehicle, with both fuel cell and energy storage system. Moreover, this case would allow a more realistic study, due to the fact that the storage systems could absorb regenerative braking, which was not tested

by Moore.

Nonlinear dynamic model for fuel cells

4.1. Introduction

This chapter presents a nonlinear dynamic model of PEM fuel cells for simulation purposes, in both absolute and relative (per-unit) units, its deduction, development and validation.

A PEM fuel cell is an electrochemical system which produces the electric power through its principal component: the stack. But the stack needs auxiliary systems, such as fan, compressor, filter, etc. in order to keep the stack environment in the correct operating conditions. Hence, the PEM fuel cell behavior presents thermal effects due to the heat generation, fluid dynamics present by the water and gas transport, electrochemical reactions in the stack, electrical phenomena, etc. The fluid, thermal and electrochemical approach are specially useful for the development stage of fuel cells. But for its integration in its final application it is more useful an electric model, which can easily interact with the rest of electric models: electric machines, grid, power converters, etc.

Therefore, in this Thesis an electric model will be developed. This elec-

tric model will adopt the form of an equivalent circuit which will be able to reproduce its voltage dynamic performance. The parameters of the resulting equivalent circuit will be obtained through electrochemical impedance spectroscopy EIS tests. Although the work is applied to a PEM fuel cell, the experimental methodology and results can be extended to other technologies such as SOFC, DMFC, PAFC, etc.

The PEM fuel cell studied is a 1.2 kW Nexa Ballard fuel cell which operates with direct gaseous hydrogen at its anode and air at its cathode [28]. Its principal characteristics are detailed in Fig. 4.1 and Fig. 4.2, and Fig. 4.3 presents its photograph. The Nexa fuel cell presents the particular characteristic of being a closed system, in which the user can only control the current output, but not the auxiliary services: pump, fan, etc. To do that it would have been necessary to modify the hardware of the control system by cutting wires and soldering new components to the printed circuit. Obviously this operation would have invalidated the product warranty. Therefore, the model presented does not control the auxiliary services, as this is done by the onboard fuel cell control system. If this can be a disadvantage for control purposes, it turns into an advantage taking into account that most commercial fuel cells are also closed loop systems. This is specially beneficial for safety reasons.

4.2. EIS tests experimental procedure

Electrochemical Impedance Spectroscopy EIS is an experimental procedure carried out in the frequency domain, in which either the current or voltage of the tested element is controlled, their ratio being represented by an electrical impedance, as explained in more detail in the State-of-the-art chapter.

Due to the fact that the fuel cell current is more easily controlled than voltage, galvanostatic (current control) mode tests are conducted. In this mode the fuel cell is set to its dc operation current and a small signal ac current with variable frequency is superimposed. Both the dc+ac current components cause a dc+ac voltage response, which allows the obtention of

OUTPUTS	Requirement	Definition	Quantity
Power1	Rated Power	Capacity at Standard Conditions, BOL	1200 W
Voltage	Operating voltage range	22 V to 50 V	
Voltage at Rated Power	26 V		
Start-up Time	Min. time to Pn from a Cold Start	2 minutes	
Emissions	Noise	Maximum noise emission at 1m	72 dBA
Water	Max. water produced at Pn	870 mL/hr	
Physical	Dimensions	L x W x H	56 x 25 x 33cm
Mass	Total system mass	13 kg	
Lifetime	Operating Life	Minimum number of operating hours before EOL	1500 hours
Cyclic Life	Min. n ^o start and shut-down cycles before EOL	500	
Shelf Life	Min. storage before EOL	2 years	
INPUTS	Requirement	Definition	Quantity
Fuel	Purity	Lowest acceptable concentration of hydrogen	99.99% H2 (vol)
Pressure	Allowable inlet supply pressure	70 – 1720 kPa(g)	
Acceptable Impurities	Max. inert fluids	0.01% (vol)	
Maximum CO and CO2 combined	2 ppm (vol)		
Maximum total hydrocarbon	1 ppm (vol)		
Maximum oxygen	500 ppm (vol)		
Consumption	Max. fuel consumption at Pn	less than 18.5 SLPM	
Power Conditioning	Current Ripple	Max. current ripple at 120 Hz	24.7% RMS 35% pp
DC Power	Voltage	Allowable range of input voltage	18 V to 30 V
Supply	Power	Maximum power draw during start-up	60 W
Operating	Location	Acceptable locations for use	Indoors and outdoors
Environment	Temperature Range	Acceptable ambient, cooling and oxidant air T ^o	3°C - 40°C
Relative Humidity	Acceptable ambient relative humidity	0% - 95% (non-condensing)	
EMI Tolerance	Operates safely in the EMI environment	specified by UL 991	

Fig. 4.1: Characteristics of the Nexa fuel cell

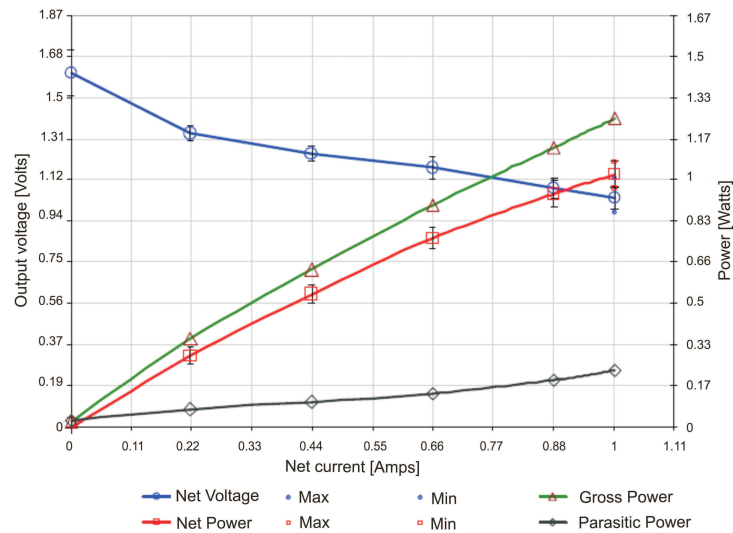
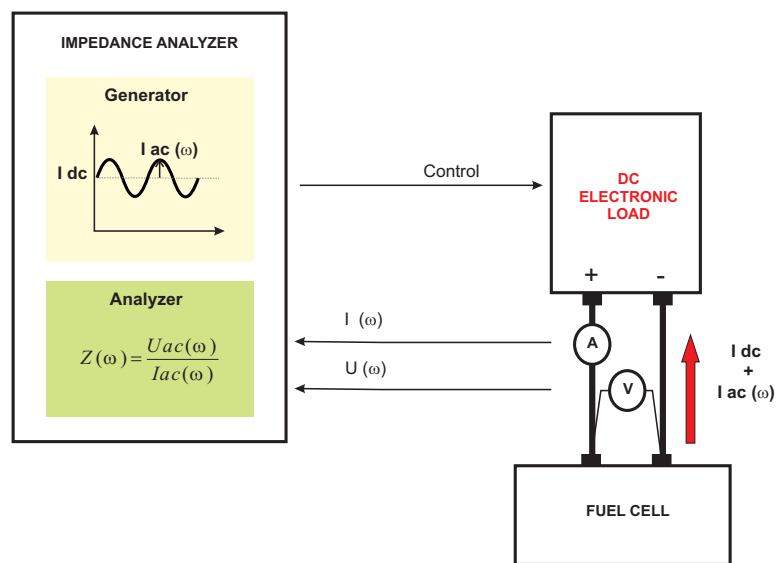


Fig. 4.2: Nexa fuel cell characteristic curve [28]



Fig. 4.3: Nexa fuel cell used


 Fig. 4.4: *EIS* on fuel cells

the battery complex impedance taking into account only the ac components of the current and voltage signals, as depicted in Fig. 4.4.

4.2.1. DC operation conditions

In this Thesis EIS tests were carried out for different output currents ranging from 10 to 50 A. According to the operational manual [28] the tests could be performed up to 60 A. However, at 50 A the fan and air pump duty cycle were already near 95 %, hence, this value has been chosen as a practical current limit. The tests were carried out after 1 h of continuous operation in the working point owing to the slow dynamics. To reach the steady-state

situation the fuel cell needs a certain amount of time for the membrane to hydrate adequately and to reach the operation temperature. Obviously, this time depends on the current programmed. For low currents, the steady-state regime is reached more quickly due to the relatively small temperature increase. Higher currents increase the water generation at the cathode and cause higher stack temperatures, and therefore the fuel cell needs a longer time to reach its humidity, temperature and voltage steady-state regime. Other authors wait up to 5 h, as [58].

During the tests the anode of the fuel cell was fed with hydrogen at 11 bar (from a 200 bar bottle by means of a pressure regulator). As the Nexa fuel cell is provided with a communications board and its own software, an external 24 V power supply was needed.

4.2.2. AC test conditions

As seen in Fig. 4.5, for each operation point an ac component is superimposed. The amplitude of the ac component must not disturb the linearity hypothesis which is supposed during the tests. In order to calculate the impedance it is necessary to suppose that current and voltage have a linear relationship during each EIS test. However, the final model obtained is not linear, due to the fact that voltage does not vary lineally with current, as depicted in Fig. 4.5. The sinusoidal ac superimposed current can admit different amplitude values, however, it should not be too high as it would alter visibly the dc operation point, nor too small as it would be confounded with the noise present in the signal. Yuan [55] investigated different amplitude values and finally selected a 5% of the dc current because other values distorted the Nyquist plot, as explained during the state-of-the-art. Following the recommendation done by Yuan, in this Thesis we also apply an ac signal with an amplitude of a 5% of the dc current.

The ac signal frequency sweep can be as wide as desired, e.g. from mHz to MHz. The frequency interval is limited by the test time and the test purpose. If the lower frequency limit is very low, the test time would lengthen and the test conditions (fuel cell humidity, temperature, etc.) would vary from